

OpenEarthAgent : A Unified Framework for Tool-Augmented Geospatial Agents

Akashah Shabbir^{1*}, Muhammad Umer Sheikh^{1*}, Muhammad Akhtar Munir¹,
Hiyam Debary², Mustansar Fiaz², Muhammad Zaigham Zaheer¹, Paolo Fraccaro²,
Fahad Shahbaz Khan^{1,3}, Muhammad Haris Khan¹, Xiao Xiang Zhu⁴, and
Salman Khan^{1,5}

¹ Mohamed bin Zayed University of Artificial Intelligence

² IBM Research

³ Linköping University

⁴ Technical University Munich

⁵ Australian National University

 <https://github.com/mbzuai-oryx/OpenEarthAgent>

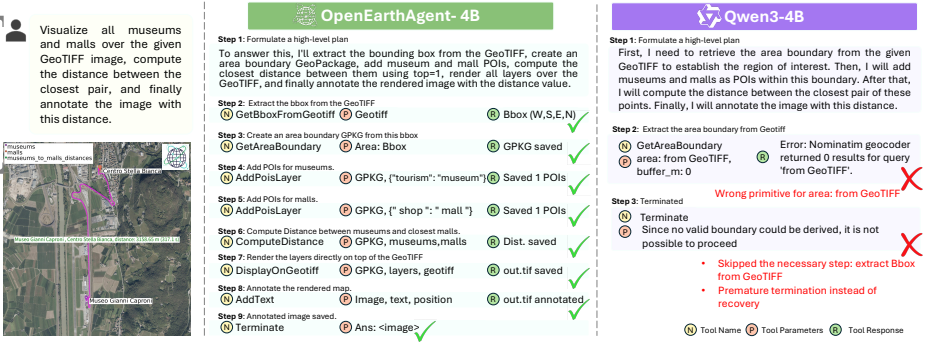


Fig. 1: Comparison of OpenEarthAgent-4B and Qwen3-4B on a complex GIS reasoning task. OpenEarthAgent correctly sequences tool calls with proper dependencies and feedback, while Qwen3 fails due to misordered tool usage and inconsistent reasoning.

Abstract. Recent progress in multimodal reasoning has enabled agents that interpret imagery, connect it with language, and execute structured analytical tasks. Extending these capabilities to remote sensing remains challenging, as models must reason over spatial scale, geographic structures, and multispectral indices while maintaining coherent multi-step logic. To address this gap, we introduce *OpenEarthAgent*, a unified framework for tool-augmented geospatial reasoning trained on satellite imagery, natural-language queries, and structured reasoning traces. Beyond serving as a benchmark, OpenEarthAgent establishes a cohesive agentic architecture built around a unified executable tool registry and trajectory-based policy learning. The framework standardizes heterogeneous visual, spectral, GIS, and georeferenced raster operations under

* Equal contribution.

a consistent callable schema, enabling modular orchestration and deterministic execution. Training is performed via supervised fine-tuning on structured reasoning trajectories with deterministic replay validation to ensure executability and spatial correctness. The accompanying corpus comprises 14,538 training and 1,169 evaluation instances with over 107K reasoning steps, spanning urban, environmental, disaster, and infrastructure domains and incorporating GIS operations alongside index analyses such as NDVI, NBR, and NDBI. Grounded in explicit reasoning traces, the learned agent demonstrates structured reasoning, stable spatial understanding, and interpretable tool-driven behaviour across diverse EO scenarios. We report consistent improvements over a strong baseline and competitive performance against recent open and closed-source models. Our code and trained models will be publicly available.

1 Introduction

The evolution of visual representation learning has transitioned from static perception to interactive multi-modal reasoning. Early single-shot frameworks such as DINO [3] and MAE [13] laid the foundation for large-scale visual understanding through self-supervised objectives, learning strong image encoders without explicit language-based reasoning or interaction. Inspired by these successes, the remote sensing community extended this paradigm to earth observation, where models such as Prithvi [15], Copernicus-FM [40], Galileo [36], Panopticon [37], TerraFM [6], and AnySat [1] scaled representation learning to global multisensor data. These earth-scale vision models demonstrated remarkable transfer across spatial resolutions and modalities, yet their predictions remained one-shot and perception-centric, focusing on recognition rather than structured reasoning.

In parallel, large multi-modal models have progressed beyond perception. Architectures such as BLIP-2 [18], InstructBLIP [5], LLaVA-OneVision [17], and Kosmos-2 [27] extended language models into the visual domain, enabling grounded image understanding. Building on this trajectory, remote-sensing VLMs emerged to adapt multimodal reasoning to geospatial data. Early efforts such as RemoteCLIP [21], SkySenseGPT [23], and GeoChat [16] introduced large-scale multimodal alignment for remote sensing through paired image–text and instruction-following datasets. Recently, EarthDial [31] advanced this paradigm by extending grounding across optical, SAR, thermal, and temporal modalities, enabling unified multimodal reasoning for classification, captioning, and change analysis. Despite coupling language with perception, current remote sensing VLMs remain largely descriptive and lack explicit structured reasoning.

Subsequent reasoning-centric approaches such as ReAct [47], DeepSeek-R1 [10], and VLM-R1 [30] introduced structured planning and, in some cases, tool-driven reasoning, transforming static perception into organized multi-step task execution. Recent developments such as OpenThinkIMG [33] unified these advances through multi-step vision-tool interaction, where large vision-language models iteratively “*think with images*” through executable reasoning trajectories. Inspired by these advances, efforts such as ThinkGeo [29] and Earth-Agent [7]

began exploring tool-augmented reasoning for earth observation (EO). They demonstrate that large models can plan analytical chains but still face challenges in geospatial grounding, coordinate consistency, and physically verifiable outputs. These limitations highlight the need for geographically grounded agents that integrate perception with explicit and interpretable reasoning.

Building on this motivation, we construct a comprehensive agentic corpus and training framework that integrates GIS-based layers, index-driven computations, and multisensor imagery, including both optical and SAR modalities, to support a wide spectrum of EO reasoning tasks. Our dataset comprises training image-query reasoning-trace instances, along with a held-out evaluation set designed to benchmark model consistency and reasoning performance across diverse geospatial scenes. The data span diverse contexts, including urban infrastructure, environmental monitoring, disaster assessment, land-use mapping, and transportation analysis, and incorporate GIS operations (e.g., distance, area, zonal statistics) alongside index-based analyses such as NDVI, NBR, and NDBI. Each sample provides an explicit reasoning trajectory linking multiple tool calls, intermediate states, and outcomes, enabling agents to learn structured, interpretable workflows rather than static predictions.

Central to this design is a unified tool registry that abstracts heterogeneous geospatial operators through a standardized executable schema, enabling consistent orchestration across perception, GIS computation, spectral analysis, and georeferenced raster reasoning. Unlike prior EO benchmarks that focus primarily on data scale, our contribution lies in coupling the dataset with an execution engine and trajectory-based policy alignment. This integration ensures that reasoning steps are not only generated but deterministically validated for spatial and logical consistency. To assess generalization and reasoning fidelity, we benchmark a broad suite of large and reasoning models, including the GPT family [25], Qwen [46], InternLM [2], and other recent multimodal LLMs. Our dataset is constructed through a unified data-gathering pipeline, where each modality undergoes question synthesis and automated validation to ensure reasoning diversity, spatial grounding, and cross-source consistency. This large-scale, tool-augmented corpus bridges the divide between GIS analysis and remote-sensing perception, providing a unified setting for evaluating structured geospatial reasoning. This work introduces an agentic framework for remote sensing that integrates tool-based reasoning within a unified training and evaluation setup.

Specifically, our key contributions are:

- **Unified data-construction pipeline:** A systematic process integrating multisensor imagery (RGB, SAR), GIS layers, and index-based computations through question synthesis and automated validation.
- **Agentic reasoning framework with deterministic validation:** A unified tool registry and a trajectory-based supervised alignment mechanism that enforces consistent tool syntax, executable reasoning chains, and spatially grounded decision-making (Fig. 1).

- **Comprehensive multimodal corpus:** 14,538 training instances and 1,169 evaluation tasks establishing a benchmark for studying spatial reasoning, grounding, and interpretability across reasoning and non-reasoning models.

2 Related Work

Remote sensing has progressed from task-specific models to large-scale foundation and vision-language models trained on global, multimodal data. Early self-supervised methods [4, 24] established transferable pretraining strategies on Sentinel archives. Subsequent foundation models include Prithvi-v2 [35] with spatiotemporal transformers on HLS, Copernicus-FM [40] with metadata-aware hypernetworks for Sentinel, Panopticon [37] and AnySat [1] with spectral- and resolution-adaptive embeddings, and CROMA [8] fusing radar and optical contrastive learning. Galileo [36] captures global-to-local context, demonstrating scalable pretraining across diverse sensors and geographies. On the multimodal side, GeoChat [16] enabled language grounding to satellite imagery, and EarthDial [31] extended this paradigm to multi-resolution optical, SAR, thermal, and temporal modalities across diverse tasks. Despite their scalability and representational strength, these models remain largely single-pass encoders; they lack structured reasoning, tool orchestration, and verifiable intermediate analysis.

Alongside foundation models, agentic systems have emerged that couple reasoning with external tools and feedback-driven control. Early frameworks such as ReAct [47] and Voyager [39] demonstrated the transition from static inference to autonomous, goal-directed reasoning. Subsequent systems, including WebAgent [42], VisTA [14], and DeepEyes [50], introduced modular architectures capable of selecting and sequencing tools under guided supervision, improving reasoning depth and execution consistency. OpenThinkIMG [33] unified these ideas through large-scale visual-tool integration with standardized APIs, while OctoTools [22] emphasized modular, verifiable execution via structured tool interfaces. Collectively, these systems established key principles: looped reasoning, standardized tool I/O, and trajectory-based learning, yet remain geospatially naive, lacking coordinate awareness, scale handling, and domain-specific spatial verification essential for earth observation analysis.

An emerging wave of EO research is now bringing these agentic principles into geospatial contexts. ThinkGeo [29] frames EO QA as tool-augmented reasoning, benchmarking ReAct-style chains and exposing persistent weaknesses in coordinate consistency, spatial grounding, and multi-step planning. Earth-Agent [7] broadens the tool ecosystem to include spectral products and standardized interfaces but still relies on largely predefined workflows, limiting physically verifiable GIS and index-based reasoning. Geo-OLM [32] explores plan-tool-verify prompting for compact models, improving efficiency but depending primarily on prompt-level heuristics rather than learned adaptive policies. Building on this gap, we introduce an EO-native agentic stack that unifies dataset construction, supervised reasoning alignment, and evaluation under a physically grounded framework. OpenEarthAgent enables broad orchestration of GIS, index-based,

Table 1: Comparison of geospatial/EO agent frameworks. Abbrev.: RS=remote sensing; MM=multimodal inputs; Tools=executable tool/function calls; MS=multi-step reasoning; GIS=GIS/vector-raster geospatial; Spec=spectral (e.g., indices, multi-spectral); CD=change detection; RData=reasoning-supervision data for training.

Method	RS	MM	MS	GIS	Spec	CD	RData
ReAct [47]	✗	✗	✓	✗	✗	✗	✗
OpenThinkIMG [33]	✗	✗	✓	✗	✗	✗	✓
ThinkGeo [29]	✓	✓	✓	✗	✗	✓	✗
Earth-Agent [7]	✓	✓	✓	✓	✓	✗	✗
Geo-OLM [32]	✓	✗	✓	✗	✗	✗	✗
RS-Agent [45]	✓	✗	✗	✗	✗	✗	✗
RS-ChatGPT [11]	✓	✗	✗	✗	✗	✗	✗
OpenEarthAgent (Ours)	✓	✓	✓	✓	✓	✓	✓

optical, and SAR operations through structured instruction-tool pairs; trains on detailed reasoning traces with a dedicated evaluation set; and supports interpretable, verifiable, multi-step reasoning across diverse geospatial conditions.

3 OpenEarthAgent

3.1 Dataset Curation

We curate a large-scale remote-sensing dataset linking imagery, queries, and tool-based reasoning traces to enable interpretable, multi-step geospatial analysis.

Overview and Motivation: The dataset presented in this work serves as a foundation for training and evaluating tool-augmented geospatial reasoning agents. While recent EO datasets primarily focus on visual classification or retrieval, they lack explicit reasoning structure and tool-level traceability. Our dataset bridges this gap by integrating imagery, natural-language queries, reasoning traces, and tool executions in a unified schema. It aims to teach models not only to recognize patterns in satellite data but also to plan, verify, and compute through structured analytical workflows. A comparative overview against existing agent frameworks is provided in Table 1, highlighting differences in modality coverage, tool integration, reasoning depth, and supervision design. In total, it contains 14,538 training samples and 1,169 held-out test samples for benchmarking, covering diverse geographic regions, sensor modalities, and reasoning tasks designed for interpretable multi-step learning and evaluation.

Data Sources and Composition: The dataset integrates heterogeneous imagery and metadata from open-access EO repositories, encompassing optical, SAR, GIS, and multispectral domains. Primary sources include high-resolution benchmarks such as DOTA [43], DIOR [19], xBD [12], AID [44], NWPU-VHR-10 [38], FloodNet [28], and Global-Dumpsite [34], complemented by Sentinel collections and Google Earth Engine archives (see Table 2 for details). Each dataset offers distinct spatial resolutions and annotation formats (bounding boxes, segmentation masks, category labels), providing both fine-grained object understanding and large-scale semantic context. The collection spans seven thematic

Table 2: Comprehensive overview of data sources used for dataset construction, across optical, SAR, GIS, and multispectral domains. These sources provide complementary spatial resolutions and annotations, ranging from urban and transport monitoring to environmental and disaster assessment, forming a rich foundation for multi-sensor, tool-based geospatial reasoning. GSD = ground sample distance, B-Box = bounding box, Seg. = segmentation.

Source	Annotation Type	Sensor (m/px)	Year	Applications / Tasks
OPTICAL DATASETS				
DIOR [19]	B-Box, Category	0.5–30	2024	Transport & Aviation Monitoring; Infrastructure Mapping
DOTA [43]	GSD, B-Box, Category	0.1–1	2021	Transport Surveillance; Infrastructure Assessment
NWPU-VHR-10 [38]	B-Box, Category	0.5–2	2023	Aviation; Transport; Infrastructure
UCAS-AOD [51]	B-Box, Category	0.5–2	2015	Aviation; Transport
AID [44]	B-Box, Category	0.2–2	2017	Urban Planning; Industrial Site Detection
iSAID [41]	GSD, B-Box, Seg. Map, Pix. Count	0.1–1	2019	Segmentation; Transport Monitoring
xBD [12]	GSD, B-Box, Category, Pix. Count	1–3.5	2019	Disaster Assessment; Change Detection
FloodNet [28]	GSD, B-Box, Category, Seg. Map, Pix. Count	0.015–0.02	2020	Flood Monitoring; Damage Estimation
Global-Dumpsite [34]	B-Box, Category	0.3–0.8	2023	Environmental Monitoring; Waste Localization
SAR DATASETS				
SSDD [49]	B-Box, Category	1–15	2021	Ship Detection; Maritime Transport
SADD [48]	B-Box, Category	0.5–3	2022	Aviation; Vessel Identification
SIVED [20]	B-Box, Category	0.1–0.3	2023	Vehicle Detection; Transport Monitoring
GIS-BASED SOURCES				
OpenStreetMap [26]	POIs (Points of Interest)	N/A	2017-	Urban Mapping; Infrastructure Analysis
INDEXED / MULTISPECTRAL SOURCES				
GoogleEarthEngine [9]	Index Layers	10–30	2017-	Urban Planning; Change Detection; Environmental Monitoring

domains: *urban planning, disaster assessment, environmental monitoring, transportation, aviation, recreation, and industrial infrastructure*. Multispectral and indexed layers (e.g., NDVI, NBR, NDBI) are derived through Google Earth Engine to complement optical and SAR imagery with physically meaningful environmental indicators. Where required for spatial reasoning tasks, samples are associated with geospatial metadata such as coordinates, projection reference, and ground sampling distance (GSD), enabling verifiable geospatial analysis.

Automated Curation Pipeline and Quality Control: Dataset construction begins by aggregating candidate regions, annotations, and metadata from multiple geospatial sources. For RGB-SAR branches, a *Sample Sufficiency Filter* module removes datapoints that do not meet the required annotation counts, after which an *Annotation Harmonizer* module aligns labels across source datasets to produce a unified annotation format. Index-based samples are mined by de-

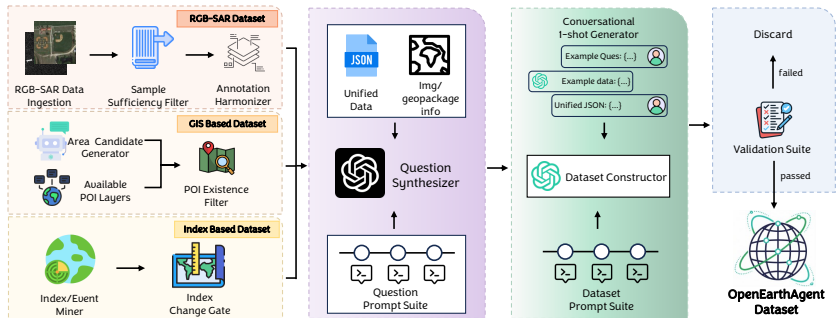


Fig. 2: Unified data-curation pipeline for the OpenEarthAgent dataset. RGB/SAR imagery, GIS spatial layers, and index-driven datasets are processed through dedicated filtering (annotation checks, POI constraints, and spectral-change signals such as NDVI/NBR/NDBI). The resulting samples are merged into unified JSON records with imagery metadata and geopackage information. A question synthesizer and conversational generator produce tool-grounded queries and reasoning traces, which are automatically validated to ensure geographic and syntactic correctness before forming the final corpus for agentic training and evaluation.

tecting temporal variations in spectral indicators such as vegetation loss, burn severity, or flooding. All sources are converted into a unified JSON schema encapsulating imagery paths, GeoPackage metadata, spatial attributes, and tool arguments. Before the final generation, candidate GIS queries are programmatically executed (e.g., POI counting, distance computation, area estimation) to verify argument correctness and prevent formatting inconsistencies. Potential inconsistencies such as mismatches between query instructions and tool parameters or invalid execution outputs are automatically detected, followed by controlled regeneration and targeted manual verification when necessary.

Natural-language queries and corresponding reasoning trajectories are synthesized through a structured LLM-driven module. We curate prompt templates per task type and employ one-shot exemplars tailored to each reasoning category. Once finalized, the data generator produces complete entries that contain queries, multimodal inputs, and serialized reasoning traces. Each instance is validated by executing the corresponding tool calls to verify argument correctness, geometric validity, and spatial consistency. All test-set samples additionally pass manual inspection to ensure realistic geospatial measurements (e.g., correcting GSD inconsistencies that may produce unrealistic area estimates). Validated samples are incorporated into the final corpus. A summary of the pipeline is shown in Fig. 2.

Task Structure and Query Design: Each instance represents a query-driven reasoning process that transforms static observation into an iterative perception-action loop (see Fig. 3). Queries are expressed in natural language and paired with structured reasoning traces that interleave *thoughts*, *actions*, and *observations*, ultimately converging on a final *answer*. These traces span diverse modalities and task types, including: GIS operations (distance, buffer, area, zonal

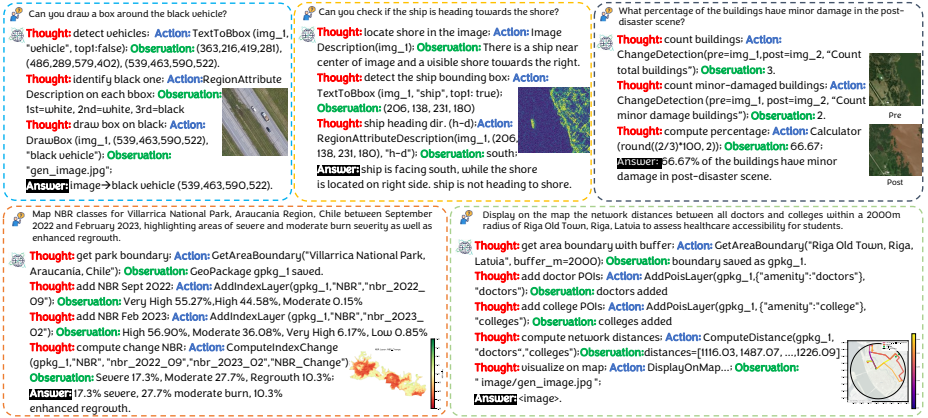
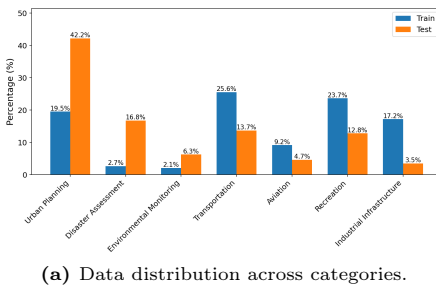
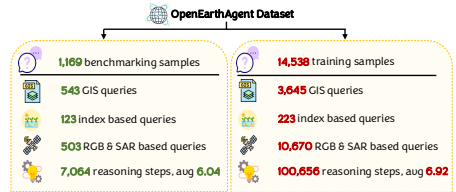


Fig. 3: Representative query-reasoning trajectories from dataset, showing interleaving of natural-language thoughts, tool executions, and observations across tasks such as object localization, direction estimation, spectral mapping, change detection, and GIS-based analysis. Examples are *simplified excerpts* of longer multi-step reasoning traces.



(a) Data distribution across categories.



(b) Key statistics for the curated corpus used for training and evaluation of our proposed agentic pipeline.

Fig. 4: Dataset overview: category distribution (left) and corpus statistics (right).

statistics), object-level reasoning (counting, comparison, orientation, proximity), spectral index computation (NDVI, NBR, NDBI), and temporal change detection. Reasoning depth and tool sequence length vary across samples, but each trajectory provides a complete chain of intermediate steps, enabling transparent multi-step geospatial problem solving rather than one-shot prediction.

Dataset Statistics: Fig. 4 summarizes the scale, distribution, and structure of the OpenEarthAgent dataset. The training split contains 14,538 instances, and the benchmark split contains 1,169 evaluation samples, each with multimodal imagery, a natural-language query, and a structured reasoning trace with interleaved tool calls and intermediate observations. The training set contains 100,656 reasoning steps (average 6.92 per query), and the benchmark split contains 7,064 reasoning steps (average 6.04 per query). Reasoning steps correspond to explicit thought-action-observation transitions, while tool calls capture the diversity of operational pathways required for solving curated agentic tasks. The breadth

of modalities, thematic coverage, and depth of reasoning traces enable rigorous evaluation of grounded, interpretable, and tool-augmented geospatial reasoning.

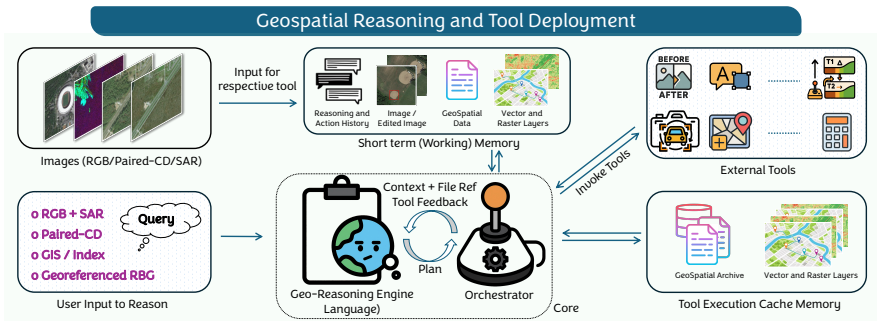


Fig. 5: Overview of the proposed *OpenEarthAgent* framework. The figure depicts tool deployment, where user queries over RGB, SAR, paired change-detection (CD), or GIS/indexed imagery are processed by the geospatial reasoning engine and tool orchestrator, which invoke appropriate tools and integrate feedback.

3.2 Methodology

Overview: We present *OpenEarthAgent*, a unified agentic learning framework for multimodal reasoning over earth observation data. The framework integrates tool-driven interaction and language-grounded reasoning into a single end-to-end formulation. Unlike conventional, single-step multimodal models, *OpenEarthAgent* decomposes geospatial reasoning into an organized sequence of perception and action steps, where the agent learns to *perceive*, *reason*, and *act* through callable tools operating on visual, textual, and spatial modalities. Given a natural-language instruction \mathbf{u} and corresponding multimodal inputs \mathbf{v} (e.g., RGB imagery, paired change-detection inputs, SAR, GIS layers, or georeferenced raster data), the agent generates multi-step reasoning trajectories that interleave internal thoughts with explicit tool invocations and their returned outputs (see Fig. 5). At each step, the agent maintains a short-term working memory that contains: instructions, observations, prior tool calls, spatial metadata, and contextual feedback from previous executions, which enable iterative reasoning and consistent spatial grounding. Training follows a supervised fine-tuning procedure on validated reasoning traces, improving syntactic validity, spatial consistency, and multi-step reasoning coherence across diverse geospatial contexts.

Unified Tool Registry: To standardize the diverse operators used in EO reasoning, we construct a unified tool registry that abstracts heterogeneous visual, spectral, and GIS operations through a consistent callable schema:

$$\mathcal{M}_j = (\mathbf{x}_{\text{in}}, \mathbf{y}_{\text{out}}, \psi_j), \quad (1)$$

where \mathbf{x}_{in} denotes structured input arguments, \mathbf{y}_{out} denotes structured outputs, $\psi_j : \mathbf{x}_{\text{in}} \mapsto \mathbf{y}_{\text{out}}$ is the executable function implementing the operation. All tools follow standardized JSON-based contracts to ensure consistent serialization and validation across training and inference. A central orchestrator parses model-generated tool calls, validates arguments, executes ψ_j , and appends returned outputs to the working memory. During execution, a predicted tool invocation s_t with arguments $\hat{\mathbf{x}}_t$ is evaluated as $\mathbf{y}_t = \psi_{s_t}(\hat{\mathbf{x}}_t)$, and the returned output \mathbf{y}_t becomes part of the updated reasoning context.

To ensure efficiency and consistency, intermediate outputs (e.g., derived vector layers, raster subsets, index maps, computed geometries) are stored in a tool execution cache memory. This cache includes geospatial archives and vector/raster layers that can be reused by subsequent tool calls within the same trajectory. Caching prevents redundant computation and ensures deterministic replay of reasoning steps. New tools can be integrated by registering their schema \mathcal{M}_j without retraining the backbone model, ensuring extensibility while maintaining interface consistency. We outline the tool categories:

a) Perceptual Tools. These operators ground language into image-space entities. `TextToBbox`, `ObjectDetection`, and `RegionAttributeDescription` convert free-form queries into spatial primitives such as bounding boxes and semantic tags. `CountGivenObject` and `SegmentObjectPixels` support object counting and pixel-level area estimation. `ChangeDetection` analyzes multi-date imagery to detect structural changes such as damage or flooding. **b) GIS Computation Tools.** These tools enable geographic reasoning through geometric and coordinate-aware computation. Operators such as `GetAreaBoundary`, `AddPoisLayer`, and `ComputeDistance` manipulate vector geometries within standard coordinate reference systems. Outputs include numerical measures (e.g., distances, buffers, zonal statistics) or derived layers visualized via `DisplayOnMap`. **c) Spectral Tools.** These operators perform band arithmetic and spectral analysis on raster inputs. `AddIndexLayer`, `ComputeIndexChange`, and `ShowIndexLayer` compute and visualize indices such as NDVI, NBR, and NDBI. They enable quantitative reasoning over environmental dynamics. **d) Georeferenced Raster Tools.** Tools such as `GetBboxFromGeotiff` and `DisplayOnGeotiff` operate directly on georeferenced rasters. They support coordinate extraction, bounding box derivation, and visualization aligned with spatial metadata, ensuring spatial consistency. **e) Utility Tools.** Utilities such as `Calculator`, `Solver`, and `Plot` support arithmetic and symbolic reasoning. Visualization tools `DrawBox` and `AddText` display intermediate results. `OCR` and `GoogleSearch` extend multimodal understanding through text extraction and contextual retrieval. `Terminate` signals completion of a reasoning trajectory.

Reasoning Trajectories and Training Objective: Each training sample encodes a structured reasoning trajectory that connects an instruction \mathbf{u} , observations \mathbf{v} , and a sequence of tool interactions. Formally, the trajectory is

represented as:

$$\begin{aligned} \Gamma_i &= \{(s_t, r_t)\}_{t=1}^{T_i}, \quad s_t \in \mathcal{S}, \\ r_t &\sim \mathcal{E}(s_t \mid \mathbf{u}_i, \mathbf{v}_i, \{(s_k, r_k)\}_{k < t}), \end{aligned} \quad (2)$$

where \mathcal{S} denotes the set of registered tools, \mathcal{E} denotes the execution environment (tool controller + cache), and (s_t, r_t) is the t -th action-result pair. Each s_t corresponds to a predicted tool invocation, while r_t is the structured observation returned by the environment.

The autoregressive model conditions on the full working memory state when predicting the next action. Training is performed via maximum likelihood estimation over verified trajectories, optimizing only the tool-action policy:

$$\mathcal{L}_{\text{train}} = -\frac{1}{N} \sum_{i=1}^N \sum_{t=1}^{T_i} \log P_\eta(s_t \mid \mathbf{u}_i, \mathbf{v}_i, s_{<t}, r_{<t}), \quad (3)$$

where η parameterizes the model and N is the number of training samples. Tool observations r_t are appended to the working memory as contextual inputs but are masked from loss computation and not treated as policy outputs. This formulation enforces syntactic validity of tool calls, argument correctness, sequential consistency, and spatial coherence while preserving the environment-policy separation.

Before inclusion in training, each trajectory undergoes deterministic replay through the tool controller. Re-execution verifies argument formatting, coordinate integrity, geometric validity, and full-chain executability. Through supervised fine-tuning on validated multi-step trajectories, OpenEarthAgent learns to generate syntactically correct, spatially grounded, and interpretable reasoning workflows over heterogeneous EO data.

4 Experiments

In this section, we outline implementation details, describe the two evaluation modes, define metrics used to quantify reasoning fidelity, tool effectiveness, and geospatial accuracy, and discuss key experimental results and insights.

Implementation Details: OpenEarthAgent is finetuned using Qwen3-4B-Instruct-2507 as the base model. Training was performed on LLM controller on four NVIDIA A100 GPUs (40 GB). The base model is loaded via Unsloth’s FastLanguageModel, enabling efficient multi-GPU distributed training. The model is trained for one epoch with a learning rate of 2×10^{-5} , cosine learning rate scheduling, 0.05 warmup ratio, and a batch size of 16. The maximum sequence length is set to 4096 tokens to support long-context conversational tool interactions. LLM is finetuned on conventional data, where the model alternates between text generation and tool invocation, providing tool outputs and feedback in JSON format, embedded in its user and assistant turns. Training applies response-only masking, computing loss exclusively on assistant-generated

Table 3: Step-by-step evaluation under tool-agnostic rollouts. We report accuracies: Inst.; syntactic + logical validity of actions, Tool.; correct tool selection, ArgN.; presence of required parameters, ArgV.; parameter correctness, and Summ.; correctness of the final consolidated answer. While frontier LLMs lead on summary accuracy, OpenEarthAgent attains state-of-the-art Inst./Tool./ArgN./ArgV., narrowing the gap despite a substantially smaller parameter budget.

Model	Param.	Inst.	Tool.	ArgN.	ArgV.	Summ.
FRONTIERLLMS						
gpt-5		97.54	82.69	73.28	37.28	87.02
gpt-4o		99.18	93.88	85.48	45.80	86.76
o4-mini		83.68	68.33	64.17	37.95	89.48
OPEN-SOURCELLMS						
Qwen2.5-Instruct	7B	94.08	85.51	78.46	38.00	80.08
Llama-3.1-Instruct	8B	47.07	39.30	34.11	17.49	79.08
Internlm3-Instruct	8B	44.54	38.46	27.82	13.25	29.84
Mistralv0.3-Instruct	7B	64.14	35.12	26.11	12.45	24.04
Qwen2.5-Instruct	3B	85.07	72.13	64.87	24.12	68.75
BASELINELLM						
Qwen3-Instruct-2507	4B	97.34	86.94	84.12	33.55	83.28
OPENEARTHAGENT						
OpenEarthAgent	4B	99.51	97.18	96.08	62.10	83.64

tokens, enabling accurate tool calls and structured responses without optimizing on prompt text or external tool outputs. This enables the model to establish a good grounding for tool invocation.

4.1 Baseline Evaluation

To evaluate OpenEarthAgent, we benchmark its performance against a diverse set of large language models (LLMs), encompassing both proprietary and open-source variants. The comparison includes advanced frontier models (GPT-4o and its reasoning-optimized variant o4-mini), and mid- to small-scale open-weight models, including Llama3.1 and Internlm3. All models serve as interchangeable backbones within the unified OpenEarthAgent framework. We assess performance using both step-by-step and end-to-end protocols, allowing analysis of intermediate reasoning trajectories and final task completion accuracy.

Step-by-Step Evaluation: This mode measures procedural reasoning and tool-invocation behavior without executing tools. The model is given n reasoning steps and must generate a valid action at each one based on the full interaction history. The first step is exempt from validation to allow the model to formulate an initial high-level plan before committing to concrete tool interactions. This setup isolates reasoning quality and enables focused analysis of spatial semantics, plan coherence, and geospatial context understanding.

End-to-End Evaluation: This mode tests full autonomous execution with live tool use. The model issues tool calls, forms arguments, and reasons step-by-step based on prior outputs. This captures operational robustness, error handling, and the effectiveness of linking perception to action in geospatial workflows.

Table 4: End-to-end evaluation: (i) F_1 scores for tool selection across: Perception (Per.), Operation (Op.), Logic (Logic.), and GIS (GIS.); (ii) tool-order fidelity: *AnyOrder* (multiset match, order-agnostic), *SameOrder* (exact sequence match), and *Unique* (set match, no multiplicity); and (iii) task-level Accuracy, *Ans.* for non-generative and *Gen.* for image-generation. GPT-4o attains high GIS F_1 , while OpenEarthAgent achieves strong, balanced performance with superior trajectory fidelity.

Model	Param.	F ₁ scores				Tool Order			Accuracy	
		Per.	Op.	Logic.	GIS.	AnyOr.	SameO.	Uni.	Ans.	Gen.
FRONTIERLLMs										
gpt-5		16.88	47.00	6.26	91.50	46.96	46.79	47.81	43.88	46.21
gpt-4o		44.47	66.91	35.95	95.80	50.81	50.38	55.52	39.22	77.93
o4-mini		39.48	64.93	12.38	86.51	40.12	39.95	41.49	35.18	55.17
OPEN-SOURCELLMs										
Qwen2.5-Instruct	7B	20.38	37.33	26.68	75.46	31.57	30.02	36.61	15.85	41.38
Llama-3.1-Instruct	8B	22.54	16.45	32.03	64.64	39.01	37.72	44.91	12.70	55.17
Internlm3-instruct	8B	5.50	14.21	0.51	31.47	2.22	1.88	3.16	0.24	2.76
Mistral-Instruct-v0.3	7B	6.74	10.24	15.82	17.12	2.65	2.57	2.91	0.39	5.52
Qwen2.5-Instruct	3B	15.63	16.54	11.16	35.64	9.24	8.72	12.40	1.83	24.14
BASELINELLM										
Qwen3-Instruct-2507	4B	13.86	20.95	18.35	71.82	16.00	14.71	21.47	13.72	15.86
OPENEARTHAGENT										
OpenEarthAgent	4B	58.30	56.76	51.18	98.52	67.75	67.24	72.71	45.26	75.86

Evaluation Metrics: We assess the model’s procedural reasoning with five metrics. Instance Accuracy (Inst.) measures the proportion of tool called without logical or syntactic errors; Tool Accuracy (Tool) evaluates correctness of tool selection; Argument Name Accuracy (ArgN) checks the presence of all required arguments in the generated action; Argument Value Accuracy (ArgV) verifies argument correctness; and Summarization Accuracy (SummAcc) quantifies how well the model consolidates information from prior tool calls into a coherent final response. We compute F_1 for tool selection across four functional categories: Perception (Per.), Operation (Op.), Logic (Logic.), and GIS (GIS.) to capture alignment between predicted and reference tool sets. Trajectory quality is further assessed via tool-order accuracy under increasing constraints: *Unique* checks tool-to-tool correspondence without penalizing repeated calls, *AnyOrder* requires all tools (including duplicates) regardless of order, and *SameOrder* enforces both correct sequence and frequency of tool invocations. Overall task Accuracy compares final model completions with reference outputs. For image-generation tasks, success is determined by the correctness of generation tool calls and their execution success rate; all non-generation queries are evaluated by an LLM judge (gpt-4o-mini) using a standardized elaboration evaluation prompt.

4.2 Results

In step-by-step evaluation (Table 3), frontier models lead: o4-mini score highest on Summ. (89.48) while gpt4o shows strong Inst. Acc. Among open-source models, Qwen2.5-I (7B) performs competitively (Inst. 94.08, Tool. 85.51), whereas other 7B–8B models degrade, particularly on ArgV. prediction. OpenEarthAgent (4B) substantially narrows this gap despite its smaller size, achieving state-

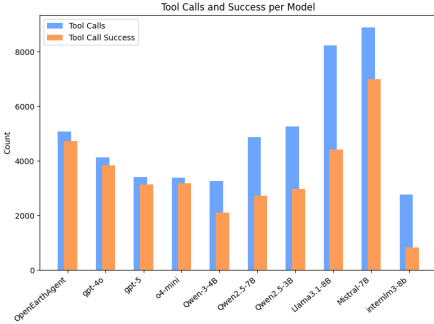


Fig. 6: Tool-call performance: Open-source models show lower success rates, while GPT family and OpenEarthAgent achieve substantially higher success rates.

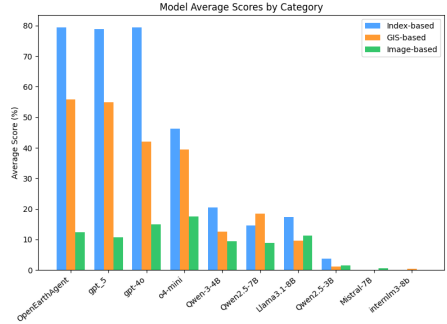


Fig. 7: Category-wise performance: OpenEarthAgent and gpt-5 lead in index/GIS score, while open source performs comparatively on image-based queries.

of-the-art Inst./ Tool./ ArgN./ and ArgV.(99.51/97.18/96.08/62.10) while substantially improving Answer Acc. (45.26). In the end-to-end evaluation (Table 4), GPT-5 avoids external logic tools and relies on internal numerical and analytical computations. GPT-4o leads in Op. F₁ (66.91) and Gen. Acc. (77.93) but remains modest in Per./Logic, whereas OpenEarthAgent delivers balanced gains across Per./ Op./Logic./GIS and dominates in tool-order accuracy (AnyOr./SameO./Uni. \approx 67-72%), indicating robust trajectory planning rather than isolated tool correctness. Overall, these results suggest that targeted training with tool schemas and trajectories can outperform larger general purpose models for geospatial tool use, especially under strict order/frequency constraints.

Tool Call & Success Patterns: Proprietary models (gpt-5, gpt-4o and o4-mini) show strong tool-control, issuing thousands of calls with low error rates (\sim 7%), indicating stable formatting. OpenEarthAgent executes a higher volume of tool calls while achieving a superior overall success rate. In contrast, open-source models such as Qwen2.5-7B, Qwen2.5-3B, and Llama-3.1-8B exhibit high failure rates (43-46%), reflecting weak adherence to the tool schema. Mistral-7B demonstrates a lower error rate but fails to invoke tools at the required adequacy to meet task demands. Despite extensive tool usage, Llama-3.1-8B and Mistral-7B fail to converge to a final answer within the allowed step, resulting in 94% and 98% incomplete task executions, respectively. Overall, performance as shown in Fig. 6 varies by call volume and precision: robust models maintain low error rates, while others struggle with consistent, well-formed tool invocations.

Category Scores: As seen in Fig. 7, OpenEarthAgent (79.43%), gpt-4o (79.39%), and gpt-5 (78.94%) achieve the strongest index-based scores, substantially outperforming all baselines. GIS-based tasks reveal a sharper degradation, with OpenEarthAgent (55.77%) followed by gpt-5 (54.94%), gpt4o (41.95%), and o4mini (39.55%). Open-source models; qwen2.5-7b, qwen3-4b, and llama3.1-8b perform comparably well on image-based queries, while smaller models approach zero on index tasks and score only marginally on GIS and image-based tasks.

Overall, the results highlight a significant performance gap and show that index- and GIS-based reasoning remains difficult for smaller open models. Additional analyses and ablations are provided in the supplementary material.

5 Conclusion

We introduced *OpenEarthAgent*, a unified framework for tool-augmented geospatial reasoning that connects natural language with multimodal earth observation data through structured analytical workflows. Unlike conventional EO models that focus primarily on perception, OpenEarthAgent performs grounded and interpretable reasoning by orchestrating visual, spectral, GIS, and GeoTIFF-aware tools under a consistent executable schema. The accompanying corpus comprises 14,538 training instances and 1,169 held-out test instances with validated multi-step reasoning trajectories, including explicit tool calls, intermediate observations, and outputs. OpenEarthAgent addresses a key gap in EO research by moving beyond perception-only modeling toward structured and verifiable geospatial reasoning. We believe this work provides a step toward agentic AI systems for environmental monitoring, disaster response, infrastructure analysis, and broader geospatial decision-making.

References

1. Astruc, G., Gonthier, N., Mallet, C., Landrieu, L.: Anysat: One earth observation model for many resolutions, scales, and modalities. In: Proceedings of the Computer Vision and Pattern Recognition Conference. pp. 19530–19540 (2025)
2. Cai, Z., Cao, M., Chen, H., Chen, K., Chen, K., Chen, X., Chen, X., Chen, Z., Chen, Z., Chu, P., Dong, X., Duan, H., Fan, Q., Fei, Z., Gao, Y., Ge, J., Gu, C., Gu, Y., Gui, T., Guo, A., Guo, Q., He, C., Hu, Y., Huang, T., Jiang, T., Jiao, P., Jin, Z., Lei, Z., Li, J., Li, J., Li, L., Li, S., Li, W., Li, Y., Liu, H., Liu, J., Hong, J., Liu, K., Liu, K., Liu, X., Lv, C., Lv, H., Lv, K., Ma, L., Ma, R., Ma, Z., Ning, W., Ouyang, L., Qiu, J., Qu, Y., Shang, F., Shao, Y., Song, D., Song, Z., Sui, Z., Sun, P., Sun, Y., Tang, H., Wang, B., Wang, G., Wang, J., Wang, J., Wang, R., Wang, Y., Wang, Z., Wei, X., Weng, Q., Wu, F., Xiong, Y., Xu, C., Xu, R., Yan, H., Yan, Y., Yang, X., Ye, H., Ying, H., Yu, J., Yu, J., Zang, Y., Zhang, C., Zhang, L., Zhang, P., Zhang, P., Zhang, R., Zhang, S., Zhang, S., Zhang, W., Zhang, W., Zhang, X., Zhang, X., Zhao, H., Zhao, Q., Zhao, X., Zhou, F., Zhou, Z., Zhuo, J., Zou, Y., Qiu, X., Qiao, Y., Lin, D.: Internlm2 technical report (2024)
3. Caron, M., Touvron, H., Misra, I., Jégou, H., Mairal, J., Bojanowski, P., Joulin, A.: Emerging properties in self-supervised vision transformers. In: Proceedings of the IEEE/CVF international conference on computer vision. pp. 9650–9660 (2021)
4. Cong, Y., Khanna, S., Meng, C., Liu, P., Rozi, E., He, Y., Burke, M., Lobell, D., Ermon, S.: Satmae: Pre-training transformers for temporal and multi-spectral satellite imagery. *Advances in Neural Information Processing Systems* **35**, 197–211 (2022)
5. Dai, W., Li, J., Li, D., Tiong, A., Zhao, J., Wang, W., Li, B., Fung, P.N., Hoi, S.: Instructblip: Towards general-purpose vision-language models with instruction tuning. *Advances in neural information processing systems* **36**, 49250–49267 (2023)

6. Danish, M.S., Munir, M.A., Shah, S.R.A., Khan, M.H., Anwer, R.M., Laaksonen, J., Khan, F.S., Khan, S.: Terrafm: A scalable foundation model for unified multi-sensor earth observation. arXiv preprint arXiv:2506.06281 (2025)
7. Feng, P., Lv, Z., Ye, J., Wang, X., Huo, X., Yu, J., Xu, W., Zhang, W., Bai, L., He, C., et al.: Earth-agent: Unlocking the full landscape of earth observation with agents. arXiv preprint arXiv:2509.23141 (2025)
8. Fuller, A., Millard, K., Green, J.: Croma: Remote sensing representations with contrastive radar-optical masked autoencoders. *Advances in Neural Information Processing Systems* **36**, 5506–5538 (2023)
9. Google Earth Engine: Google earth engine. <https://earthengine.google.com/> (2025)
10. Guo, D., Yang, D., Zhang, H., Song, J., Wang, P., Zhu, Q., Xu, R., Zhang, R., Ma, S., Bi, X., et al.: Deepseek-r1 incentivizes reasoning in llms through reinforcement learning. *Nature* **645**(8081), 633–638 (2025)
11. Guo, H., Su, X., Wu, C., Du, B., Zhang, L., Li, D.: Remote sensing chatgpt: Solving remote sensing tasks with chatgpt and visual models. In: *IGARSS 2024-2024 IEEE International Geoscience and Remote Sensing Symposium*. pp. 11474–11478. IEEE (2024)
12. Gupta, R., Hosfelt, R., Sajeev, S., Patel, N., Goodman, B., Doshi, J., Heim, E., Choset, H., Gaston, M.: xbd: A dataset for assessing building damage from satellite imagery. arXiv preprint arXiv:1911.09296 (2019)
13. He, K., Chen, X., Xie, S., Li, Y., Dollár, P., Girshick, R.: Masked autoencoders are scalable vision learners. In: *Proceedings of the IEEE/CVF conference on computer vision and pattern recognition*. pp. 16000–16009 (2022)
14. Huang, Z., Ji, Y., Rajan, A.S., Cai, Z., Xiao, W., Wang, H., Hu, J., Lee, Y.J.: Visualtoolagent (vista): A reinforcement learning framework for visual tool selection. arXiv preprint arXiv:2505.20289 (2025)
15. Jakubik, J., Roy, S., Phillips, C., Fraccaro, P., Godwin, D., Zadrozny, B., Szwarcman, D., Gomes, C., Nyirjesy, G., Edwards, B., et al.: Foundation models for generalist geospatial artificial intelligence. arXiv preprint arXiv:2310.18660 (2023)
16. Kuckreja, K., Danish, M.S., Naseer, M., Das, A., Khan, S., Khan, F.S.: Geochat: Grounded large vision-language model for remote sensing. In: *Proceedings of the IEEE/CVF Conference on Computer Vision and Pattern Recognition*. pp. 27831–27840 (2024)
17. Li, B., Zhang, Y., Guo, D., Zhang, R., Li, F., Zhang, H., Zhang, K., Zhang, P., Li, Y., Liu, Z., et al.: Llava-onevision: Easy visual task transfer. arXiv preprint arXiv:2408.03326 (2024)
18. Li, J., Li, D., Savarese, S., Hoi, S.: Blip-2: Bootstrapping language-image pre-training with frozen image encoders and large language models. In: *International conference on machine learning*. pp. 19730–19742. PMLR (2023)
19. Li, K., Wan, G., Cheng, G., Meng, L., Han, J.: Object detection in optical remote sensing images: A survey and a new benchmark. *ISPRS journal of photogrammetry and remote sensing* **159**, 296–307 (2020)
20. Lin, X., Zhang, B., Wu, F., Wang, C., Yang, Y., Chen, H.: Sived: A sar image dataset for vehicle detection based on rotatable bounding box. *Remote Sensing* **15**(11), 2825 (2023)
21. Liu, F., Chen, D., Guan, Z., Zhou, X., Zhu, J., Ye, Q., Fu, L., Zhou, J.: Remoteclip: A vision language foundation model for remote sensing. *IEEE Transactions on Geoscience and Remote Sensing* **62**, 1–16 (2024)

22. Lu, P., Chen, B., Liu, S., Thapa, R., Boen, J., Zou, J.: Octotools: An agentic framework with extensible tools for complex reasoning. arXiv preprint arXiv:2502.11271 (2025)
23. Luo, J., Pang, Z., Zhang, Y., Wang, T., Wang, L., Dang, B., Lao, J., Wang, J., Chen, J., Tan, Y., et al.: Skysensegpt: A fine-grained instruction tuning dataset and model for remote sensing vision-language understanding. arXiv preprint arXiv:2406.10100 (2024)
24. Manas, O., Lacoste, A., Giró-i Nieto, X., Vazquez, D., Rodriguez, P.: Seasonal contrast: Unsupervised pre-training from uncurated remote sensing data. In: Proceedings of the IEEE/CVF International Conference on Computer Vision. pp. 9414–9423 (2021)
25. OpenAI: Introducing gpt. <https://openai.com> (2025)
26. OpenStreetMap contributors: Openstreetmap: Collaborative project to create a free editable map of the world. <https://www.openstreetmap.org> (2025)
27. Peng, Z., Wang, W., Dong, L., Hao, Y., Huang, S., Ma, S., Wei, F.: Kosmos-2: Grounding multimodal large language models to the world. arXiv preprint arXiv:2306.14824 (2023)
28. Rahnemoonfar, M., Chowdhury, T., Sarkar, A., Varshney, D., Yari, M., Murphy, R.R.: Floodnet: A high resolution aerial imagery dataset for post flood scene understanding. *IEEE Access* **9**, 89644–89654 (2021)
29. Shabbir, A., Munir, M.A., Dudhane, A., Sheikh, M.U., Khan, M.H., Fraccaro, P., Moreno, J.B., Khan, F.S., Khan, S.: Thinkgeo: Evaluating tool-augmented agents for remote sensing tasks. arXiv preprint arXiv:2505.23752 (2025)
30. Shen, H., Liu, P., Li, J., Fang, C., Ma, Y., Liao, J., Shen, Q., Zhang, Z., Zhao, K., Zhang, Q., et al.: Vlm-r1: A stable and generalizable r1-style large vision-language model. arXiv preprint arXiv:2504.07615 (2025)
31. Soni, S., Dudhane, A., Debary, H., Fiaz, M., Munir, M.A., Danish, M.S., Fraccaro, P., Watson, C.D., Klein, L.J., Khan, F.S., et al.: Earthdial: Turning multi-sensory earth observations to interactive dialogues. In: Proceedings of the Computer Vision and Pattern Recognition Conference. pp. 14303–14313 (2025)
32. Stamoulis, D., Marculescu, D.: Geo-olm: Enabling sustainable earth observation studies with cost-efficient open language models & state-driven workflows. In: Proceedings of the ACM SIGCAS/SIGCHI Conference on Computing and Sustainable Societies. pp. 608–619 (2025)
33. Su, Z., Li, L., Song, M., Hao, Y., Yang, Z., Zhang, J., Chen, G., Gu, J., Li, J., Qu, X., et al.: Openthinking: Learning to think with images via visual tool reinforcement learning. arXiv preprint arXiv:2505.08617 (2025)
34. Sun, X., Yin, D., Qin, F., Yu, H., Lu, W., Yao, F., He, Q., Huang, X., Yan, Z., Wang, P., et al.: Revealing influencing factors on global waste distribution via deep-learning based dumpsite detection from satellite imagery. *Nature Communications* **14**(1), 1444 (2023)
35. Szwarcman, D., Roy, S., Fraccaro, P., Gíslason, P.E., Blumenstiel, B., Ghosal, R., de Oliveira, P.H., Almeida, J.L.d.S., Sedona, R., Kang, Y., et al.: Prithvi-eo-2.0: A versatile multi-temporal foundation model for earth observation applications. arXiv preprint arXiv:2412.02732 (2024)
36. Tseng, G., Fuller, A., Reil, M., Herzog, H., Beukema, P., Bastani, F., Green, J.R., Shelhamer, E., Kerner, H., Rolnick, D.: Galileo: Learning global and local features in pretrained remote sensing models. arXiv e-prints pp. arXiv–2502 (2025)
37. Waldmann, L., Shah, A., Wang, Y., Lehmann, N., Stewart, A., Xiong, Z., Zhu, X.X., Bauer, S., Chuang, J.: Panopticon: Advancing any-sensor foundation mod-

- els for earth observation. In: Proceedings of the Computer Vision and Pattern Recognition Conference. pp. 2204–2214 (2025)
38. Wang, C., Bai, X., Wang, S., Zhou, J., Ren, P.: Multiscale visual attention networks for object detection in vhr remote sensing images. *IEEE Geoscience and Remote Sensing Letters* **16**(2), 310–314 (2018)
 39. Wang, G., Xie, Y., Jiang, Y., Mandlkar, A., Xiao, C., Zhu, Y., Fan, L., Anandkumar, A.: Voyager: An open-ended embodied agent with large language models. arXiv preprint arXiv:2305.16291 (2023)
 40. Wang, Y., Xiong, Z., Liu, C., Stewart, A.J., Dujardin, T., Bountos, N.I., Zavras, A., Gerken, F., Papoutsis, I., Leal-Taixé, L., et al.: Towards a unified copernicus foundation model for earth vision. arXiv preprint arXiv:2503.11849 (2025)
 41. Waqas Zamir, S., Arora, A., Gupta, A., Khan, S., Sun, G., Shahbaz Khan, F., Zhu, F., Shao, L., Xia, G.S., Bai, X.: isaid: A large-scale dataset for instance segmentation in aerial images. In: Proceedings of the IEEE/CVF conference on computer vision and pattern recognition workshops. pp. 28–37 (2019)
 42. Wei, Z., Yao, W., Liu, Y., Zhang, W., Lu, Q., Qiu, L., Yu, C., Xu, P., Zhang, C., Yin, B., et al.: Webagent-r1: Training web agents via end-to-end multi-turn reinforcement learning. arXiv preprint arXiv:2505.16421 (2025)
 43. Xia, G.S., Bai, X., Ding, J., Zhu, Z., Belongie, S., Luo, J., Datcu, M., Pelillo, M., Zhang, L.: Dota: A large-scale dataset for object detection in aerial images. In: Proceedings of the IEEE conference on computer vision and pattern recognition. pp. 3974–3983 (2018)
 44. Xia, G.S., Hu, J., Hu, F., Shi, B., Bai, X., Zhong, Y., Zhang, L., Lu, X.: Aid: A benchmark data set for performance evaluation of aerial scene classification. *IEEE Transactions on Geoscience and Remote Sensing* **55**(7), 3965–3981 (2017)
 45. Xu, W., Yu, Z., Mu, B., Wei, Z., Zhang, Y., Li, G., Peng, M.: Rs-agent: automating remote sensing tasks through intelligent agent. arXiv preprint arXiv:2406.07089 (2024)
 46. Yang, A., Li, A., Yang, B., Zhang, B., Hui, B., Zheng, B., Yu, B., Gao, C., Huang, C., Lv, C., et al.: Qwen3 technical report. arXiv preprint arXiv:2505.09388 (2025)
 47. Yao, S., Zhao, J., Yu, D., Du, N., Shafran, I., Narasimhan, K.R., Cao, Y.: React: Synergizing reasoning and acting in language models. In: The eleventh international conference on learning representations (2022)
 48. Zhang, P., Xu, H., Tian, T., Gao, P., Li, L., Zhao, T., Zhang, N., Tian, J.: Se-fepnet: Scale expansion and feature enhancement pyramid network for sar aircraft detection with small sample dataset. *IEEE Journal of Selected Topics in Applied Earth Observations and Remote Sensing* **15**, 3365–3375 (2022)
 49. Zhang, T., Zhang, X., Li, J., Xu, X., Wang, B., Zhan, X., Xu, Y., Ke, X., Zeng, T., Su, H., et al.: Sar ship detection dataset (ssdd): Official release and comprehensive data analysis. *Remote Sensing* **13**(18), 3690 (2021)
 50. Zheng, Z., Yang, M., Hong, J., Zhao, C., Xu, G., Yang, L., Shen, C., Yu, X.: Deepeyes: Incentivizing "thinking with images" via reinforcement learning. arXiv preprint arXiv:2505.14362 (2025)
 51. Zhu, H., Chen, X., Dai, W., Fu, K., Ye, Q., Jiao, J.: Orientation robust object detection in aerial images using deep convolutional neural network. In: 2015 IEEE international conference on image processing (ICIP). pp. 3735–3739. IEEE (2015)

Supplementary

OpenEarthAgent: A Unified Framework for Tool-Augmented Geospatial Agents

Supplementary material includes ablation analysis(S1), cross-benchmark evaluation(S2), model selection criterion(S3), error analysis (S4) and context-specific performance assessment(S5). It also provides quantitative results illustrating multiple evaluation cases (S6), a detailed overview of input-output structures with corresponding tool descriptions (S7), and an evaluation prompt illustration with a comparative study on LLM Judge(S8).

S1 Ablation Analysis

Effect of Data Composition

To investigate how data composition influences model performance, we divide the training set into easy and hard subsets based on the length of reasoning trajectories, measured by the number of assistant planning and action steps in each conversation. First, samples with fewer than seven tool-calling turns are categorized as easy, while those with seven or more turns are considered hard. To avoid tool-distribution bias, we further rebalanced several underrepresented tools by evenly redistributing their samples across the two subsets. The easy subset contains 8,113 samples averaging 6.095 turns, while the hard subset contains 6,425 samples averaging 7.975 turns. We evaluated under three conditions: training on easy-only, hard-only, and combined data.

Table A1: Impact of data composition: Easy-only training achieves the best Perception score, Hard-only training boosts operational reasoning, while the combined setting yields the most balanced performance overall, achieving the highest Logic and GIS scores, the strongest tool-order consistency, and the best answer accuracy.

Data	Abl. setting		F ₁ scores			Tool Order			Accuracy		
	Easy	Hard	Per.	Op.	Logic.	GIS.	AnyO.	SameO.	Unique	Ans.	Gen.
OPENEARTHAGENT											
Set1	✓	✗	59.63	52.60	48.11	97.26	61.59	61.42	67.51	43.40	73.79
Set2	✗	✓	54.45	56.83	35.16	94.35	65.61	64.93	70.40	35.79	71.72
Set1+Set2	✓	✓	58.30	56.76	51.18	98.52	67.75	67.24	72.71	45.26	75.86

Table A1 analyzes how reasoning trajectory complexity (easy vs. hard) affects tool-selection F₁, trajectory consistency, and end-to-end task accuracy. Training on shorter trajectories (avg. 6.095 turns) yields the highest Perception F₁ (59.63) as perception tools (e.g., OCR, ObjectDetection, SegmentObjectPixels, Count-GivenObject) are typically associated with early-stage spatial grounding and visual interpretation. Shorter trajectories, therefore, provide more focused supervision on these perceptual and semantic alignment steps. Training on longer

trajectories (avg. 7.975 turns) enhances Operation F_1 (56.83) and improves tool-order robustness (AnyO 65.61, Unique 70.40). Hard samples involve extended reasoning chains and richer tool compositions, encouraging the model to learn procedural dependencies and structured multi-step workflows. However, performance in logical reasoning (35.16) remains below the combined setting low, suggesting that while challenging samples strengthen structured reasoning, they benefit from complementary, simpler cases that help stabilize reasoning chains and reinforce logical consistency across steps.

The combined setting achieves the most balanced and strongest overall performance, yielding the highest Logic F_1 (51.18) and GIS F_1 (98.52), the strongest tool-order consistency (AnyO/SameO/Unique \approx 67–73%), and the best Answer (45.26) and General Accuracy (75.86). Since GIS tools require coordinated perceptual grounding, logical inference, and sequential execution, training on the mixed dataset enhances both tool-type alignment (macro F_1 across Per./Op./Logic./GIS) and trajectory-level structural coherence. By integrating short and long reasoning traces, the model simultaneously benefits from focused perceptual supervision provided by easy samples and structured multi-step planning signals from hard samples, resulting in improved sequence fidelity under strict order and multiplicity constraints.

Comparison with In-context Learning

To evaluate the impact of in-context learning, we conduct an ablation study on Qwen3-Instruct-2507 by progressively increasing the number of in-context examples ($k \in \{5, 10, 15\}$) and comparing against the baseline model without demonstrations (BL). In-context examples are not appended as a single prompt block, but instead are prepended as a structured conversational history. Specifically, each example is injected as a sequence of user–assistant interaction turns (including intermediate thoughts, tool actions, and observations) before the actual test query. The full message list, therefore, consists of: (1) a system instruction, (2) k prior example dialogues formatted as multi-turn interactions, and (3) the target query conversation. Results are summarized in Table A2.

Table A2: Performance comparison of Qwen3-Instruct-2507 under increasing in-context example sizes ($k = 5, 10, 15$) against the baseline (BL) and OpenEarthAgent. Increasing the number of in-context examples consistently improves performance over the baseline, while OpenEarthAgent achieves the strongest results across all metrics.

Models	F_1 scores				Tool Order			Accuracy	
	Per.	Op.	Logic.	GIS.	AnyO.	SameO.	Unique	Ans.	Gen.
QWEN3-INSTRUCT-2507									
Baseline (BL)	13.86	20.95	18.35	71.82	16.00	14.71	21.47	13.72	15.86
BL+ In-context($k=5$)	20.26	37.34	30.20	87.27	29.34	28.57	31.73	26.84	44.14
BL+ In-context($k=10$)	24.86	46.29	34.02	86.54	30.88	30.28	33.28	28.73	51.72
BL+ In-context($k=15$)	34.58	42.10	37.80	89.80	36.44	36.10	39.44	33.06	46.90
OPENEARTHAGENT									
OpenEarthAgent	58.30	56.76	51.18	98.52	67.75	67.24	72.71	45.26	75.86

Adding in-context examples yields substantial improvements across all evaluation dimensions. Even with $k=5$, performance improves markedly over the baseline, particularly in Operation, GIS F_1 scores, and accuracy. Increasing k to 10 further enhances the Logical and Operation F_1 scores and yields notable gains in tool-order consistency metrics (AnyO., SameO., and Unique), suggesting that additional demonstrations help the model better internalize structured tool usage patterns.

For $k=15$, Perception and Logical F_1 scores show improvements, and tool-order metrics also consistently increase, indicating improved procedural alignment. However, degradation in Operation and Generation performance between $k=10$ and $k=15$ suggests diminishing returns beyond a certain number of demonstrations. Despite these gains, the model remains substantially below OpenEarthAgent, which outperforms all Qwen variants across every metric. This highlights that while in-context learning significantly enhances tool reasoning and execution consistency, architectural or training-level adaptations, as employed by OpenEarthAgent, are necessary to achieve state-of-the-art performance.

Tool Schema Influence

To assess the agent’s sensitivity to changes in the tool specification format (Table A3), we conduct a controlled ablation over five variants ordered from minimal structural exposure to maximal semantic conditioning.

Schema 1- Minimal Structure: This setting adds a thin layer of operational structure; a compact enumeration of all tools and a procedural rule set (e.g., one action per step, Terminate required, tool-order constraints, JSON format). No argument signatures, semantic descriptions, or usage examples are provided. This schema provides structural benefits for planning while withholding any semantic cues about the tool’s functionality. Consequently, the agent must rely on actual tool feedback to infer how each tool behaves.

Schema 2- Natural-language semantics: Global planning rules and execution constraints remain identical to Schema 1. However, high-level natural-

Table A3: Impact of Tool Schema Complexity on Model Reasoning and Tool Usage: Structural exposure (Sch.1→2) improves tool perception and selection; argument-level signatures (Sch.3) enhance interface alignment and GIS reasoning; executable constraints (Sch.4) strengthen logical consistency; and maximal specification with explicit JSON examples (Sch.5) yields the highest overall F_1 , tool-order correctness, and answer accuracy.

Tool Schema	F ₁ scores				Tool Order			Accuracy	
	Per.	Op.	Logic.	GIS.	AnyO.	SameO.	Unique	Ans.	Gen.
OPENEARTHAGENT									
Sch.1-Minimal	19.80	8.40	32.00	58.99	25.32	24.89	26.69	8.44	17.93
Sch.2-Semantic	43.53	27.24	35.80	64.71	26.96	26.45	31.58	9.10	25.86
Sch.3-Signature	48.76	28.86	34.22	76.32	26.17	25.66	29.77	12.77	40.69
Sch.4-Executable	47.01	27.91	40.94	76.86	26.55	25.95	29.26	13.03	46.21
Sch.5- Maximal	58.30	56.76	51.18	98.52	67.75	67.24	72.71	45.26	75.86

language descriptions of tool functionality are provided along with tool enumeration. The agent gains functional semantic grounding but lacks explicit demonstrations of argument structure, format exemplars, and concrete API usage patterns. This schema isolates the effect of semantic grounding without interface exemplification.

Schema 3- Compressed Signature: The third variant introduces argument level explicitness along with natural-language semantics. Tools are presented as Tool-Argument signatures, for example `ChangeDetection(text, pre_image, post_image)`. This variant provides only tool-argument information, without any detailed examples. It effectively mimics a code-completion-style API, requiring the agent to infer the tool’s behavior from the structure of the signatures.

Schema 4- Tool signature + Executable Constraint: This configuration exposes the agent to tool signatures similar to Schema 3, along with all global rules. An additional requirement is added for `command` arguments: they must contain executable Python code defining a `solution()` function, along with a single example. This operational executability constraint is critical because certain tools cannot operate without a fully defined executable function; for example, `Solver` uses `solution()` to perform symbolic reasoning using Sympy, and `Plot` returns a matplotlib figure generated by code. By enforcing executable commands, the schema ensures that the model produces actionable tool inputs for the critical tool.

Schema 5- Maximal Information: This represents the upper bound of tool-conditioning information. Each element contributes crucially: purpose-level explanations clarify the tool’s goal, argument semantics specify how inputs affect outputs, usage examples demonstrate correct application, and tool rules guide multi-step planning and sequencing. This schema enables the model to reliably understand, plan, and execute complex tool chains. The agent operates under a fully specified tool-use ontology, minimizing ambiguity.

The Table A3 shows that tool-using LLM agents are highly sensitive to how tool knowledge is structured and exposed. Performance differences arise from information exposure, specifically from the extent of semantic grounding and interface clarity. With minimal structure (Sch. 1), the model relies only on structural cues and feedback, resulting in weak reasoning and the lowest F_1 scores, particularly in perception and operation (19.80 and 8.40), indicating that the model struggles to correctly identify which tools to invoke. Introducing natural-language tool descriptions in Schema 2 (Semantic) yields a substantial improvement across F_1 metrics. Perception more than doubles (19.80 \rightarrow 43.53), and operation improves dramatically (8.40 \rightarrow 27.24). Tool-order scores also rise, suggesting that semantic grounding enables the model to better anticipate more accurate tool use and reasonable action sequences.

Adding explicit argument signatures (Schema 3) improves alignment and task-tool mapping: Perception increases (+5.23), and GIS rises substantially (+11.61), indicating stronger structural grounding. Tool-order metrics remain largely unchanged, suggesting that signature-level exposure enhances invocation

precision but not higher-level planning. Generation accuracy increases markedly (+14.83), indicating better abstraction and parameterization when invoking image-generation tools. Introducing executable constraints (Schema 4) primarily enhances reasoning rigor as seen by logical F_1 increase (+6.72). Tool-order metrics again show minimal change, indicating that executability strengthens operational validity rather than sequencing strategy.

Full specification—combining purpose descriptions, argument semantics, executable examples, and planning rules—yields the largest gains: Perception (+11.29), Operation (+28.85), Logical (+10.24), GIS (+21.66), and major improvements in tool-order correctness (AnyO. +41.20; SameO. +41.29; Unique +43.45). These improvements are primarily driven by explicit full JSON tool examples, which provide maximal interface grounding by explicitly instantiating valid invocation patterns. Compared to abstract signatures or natural-language descriptions, these examples define argument schemas, formatting constraints, required fields, quoting conventions, and executable structure. This reduces syntactic ambiguity and malformed calls under strict JSON-only constraints, thereby improving the validity of invocations, the completeness of arguments, and overall schema compliance.

Effect of Tool Order

This ablation investigates the effects of tool-list ordering and explicit procedural constraints on agent reasoning and execution behavior. We evaluate three configurations: (1) a shuffled tool list with dependency constraints preserved, (2) an optimized tool list without explicit dependency rules, and (3) an optimized tool list with explicit dependency rules enforcing valid tool calling preconditions. The first setting disrupts positional priors by randomizing the presentation of tools. The second retains a structured presentation but removes hard-coded ordering constraints, requiring the model to infer dependencies implicitly. The third combines a structured tool presentation with explicit procedural guidance.

The results (Table A4) demonstrate that tool ordering has a substantial impact on reasoning performance and execution behavior. Progressing from shuffled tool order to optimized ordering and further to optimized ordering with an explicit order rule yields consistent improvements in F_1 scores, particularly for Perception (+6.80, +1.85), Logic (+3.93, +2.68), and GIS (+2.98, +1.06). These gains indicate that structured sequencing enhances information retrieval, multi-step dependency handling, and spatial reasoning. Operational performance peaks under optimized ordering without the rule (59.54), suggesting that strict ordering constraints may marginally reduce operational flexibility.

Tool-order correctness metrics (AnyO., SameO., Unique) improve monotonically across settings, reflecting increased consistency in tool invocation patterns. Answer accuracy also improves modestly (43.35→45.26), whereas generation accuracy remains stable, indicating that ordering primarily enhances execution reliability and in-distribution reasoning rather than expanding overall generative capacity.

Table A4: Impact of Tool Order on Model Reasoning and Tool Usage: Comparing shuffled order, optimized order without rules, and optimized order with enforced pre-conditions shows consistent gains in reasoning F₁, tool-order correctness, and answer Acc., while Generation Acc. remains stable.

Tool Schema	F ₁ scores				Tool Order			Accuracy	
	Per.	Op.	Logic.	GIS.	AnyO.	SameO.	Unique	Ans.	Gen.
	OPENEARTHAGENT								
Shuffled Tool Order	49.65	58.97	44.57	94.48	63.22	62.36	67.92	43.35	75.93
Optimized Order w/o Order Rule	56.45	59.54	48.50	97.46	65.86	64.84	71.26	45.14	75.17
Optimized Order w/ Order Rule	58.30	56.76	51.18	98.52	67.75	67.24	72.71	45.26	75.86

Impact of High-Level Planning

We compare OpenEarthAgent under two configurations: (1) without high-level planning, where the agent directly invokes tools with only step-level planning, and (2) with high-level planning, where the agent generates an explicit reasoning plan prior to tool execution. Both variants are trained and evaluated on the same dataset, using identical tools, supervision, and evaluation protocols.

The results (Table A5) show that incorporating a high-level planning step leads to consistent improvements. Logical reasoning F1 increases by +3.57, reflecting improved multi-step consistency. Tool sequencing also improves, with Any-order accuracy +4.36 and Same-order accuracy +4.37, indicating more coherent and reliably structured tool execution under explicit planning. Moreover, image generation accuracy increases from 65.52 to 75.86 (+10.34), indicating that explicit high-level planning significantly improves the accuracy of deciding when to generate an image in response to a query.

S2 Cross-Benchmark Evaluation

We evaluate OpenEarthAgent on the Earth-Agent Benchmark [7] using fine-grained step-level metrics. The Earth-Agent Benchmark includes 248 tasks with 13,729 images spanning the spectrum, products, and RGB modalities. For compatibility, benchmark tools are reformatted to conform to the OpenEarthAgent interface, with additional curated JSON exemplars to standardize tool invocation and argument formatting.

Table A5: Effect of High-Level Planning: Explicit high-level planning improves logical reasoning, tool sequencing consistency, and image generation decision accuracy, leading to stronger structured execution and overall performance.

Setting	F ₁ scores				Tool Order			Accuracy	
	Per.	Op.	Logic.	GIS.	AnyO.	SameO.	Unique	Ans.	Gen.
	OPENEARTHAGENT								
w/o High-level Plan	57.74	58.82	47.61	97.11	63.39	62.87	71.77	44.50	65.52
w/ High-level Plan	58.30	56.76	51.18	98.52	67.75	67.24	72.71	45.26	75.86

Table A6: Step-by-step evaluation on Earth-Agent Benchmark.

Model	Param.	Inst.	Tool.	ArgN.	ArgV.	Summ.
FRONTIERLLMs						
gpt-4o		97.41	71.65	70.01	48.11	80.26
OPEN-SOURCELLMs						
Qwen2.5-Instruct	7B	85.98	57.76	56.06	34.66	<u>79.60</u>
Llama-3.1-Instruct	8B	83.21	55.11	54.29	35.98	73.05
BASELINELLM						
Qwen3-Instruct-2507	4B	88.32	60.61	59.53	38.89	76.79
OPENEARTHAGENT						
OpenEarthAgent	4B	<u>96.91</u>	<u>70.33</u>	<u>69.13</u>	<u>44.44</u>	79.33

As shown in Table A6, OpenEarthAgent (4B) achieves strong performance across all tool-related metrics, substantially outperforming similarly sized open-source baselines and closely matching GPT-4o. These results indicate that structured agent design and training can enable small models to achieve near-frontier performance in step-wise geospatial reasoning and tool execution.

S3 Model Selection

To determine how underlying model capacity affects tool-use accuracy and multi-step reasoning, we compare two model backbones trained under identical data, hyperparameter, and tool-conditioning settings: Qwen3-4B-Instruct-2507 and Qwen2.5-7B-Instruct. We train on 25% of the training corpus and reserve an internal 8% split from it as a held-out validation set used only for model selection, entirely separate from the benchmark test set.

Table A7: Comparison of base model performance across reasoning and tool-usage metrics. Qwen3-4B-Instruct-2507 slightly outperforms Qwen2.5-7B-Instruct. Results highlight that improved architectural alignment in the Qwen3 series yields more efficient multi-step reasoning despite a smaller model size.

Base Model	F ₁ scores				Tool Order			Accuracy	
	Per.	Op.	Logic.	GIS.	AnyO.	SameO.	Unique	Ans.	Gen.
OPENEARTHAGENT									
Qwen2.5-7B-Instruct	96.72	97.41	88.60	99.53	74.80	74.80	96.00	23.19	89.67
Qwen3-4B-Instruct-2507	97.82	97.70	91.39	99.53	81.80	81.60	97.50	23.47	90.76

As summarized in Table A7, the smaller Qwen3-4B-Instruct-2507 outperforms the 7B counterpart across nearly all metrics, particularly in logical reasoning (Logic F₁: +2.79) and tool-order consistency (AnyO: +7.0). This indicates that architectural refinements and improved alignment in the Qwen3 series enhance structured reasoning efficiency even with fewer parameters. Both variants exhibit near-saturated GIS and operational F₁ scores, confirming that tool-augmented reasoning generalizes robustly across these domains. The marginal

differences in answer and generation accuracy further suggest that reasoning quality is independent of model scale. Overall, Qwen3-4B-Instruct-2507 delivers a superior balance between model size and reasoning reliability, making it a strong candidate for a baseline model for scalable geospatial applications.

S4 Error Analysis

We conduct a fine-grained analysis of model failures to better understand where tool-augmented reasoning breaks down. Fig. A1 shows errors across 4 types, and reports their frequency across some evaluated models.

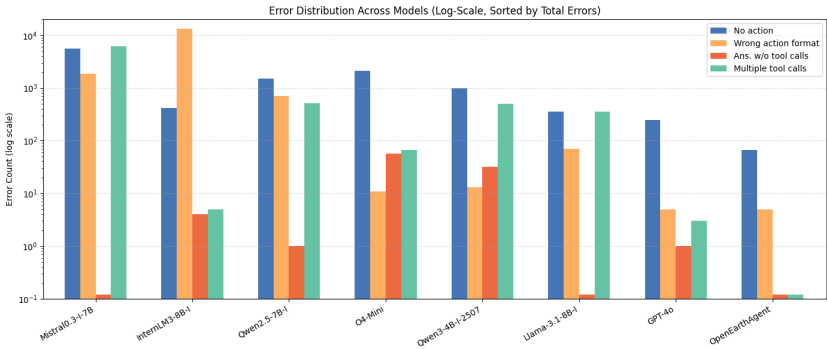


Fig. A1: Log-scale error distribution across models for four error types: No action, Wrong action format, Answer reached without a single tool call, and Multiple tool calls in a single action. Frontier models show fewer errors overall, while the fine-tuned OpenEarthAgent achieves the lowest total error count.

Syntax errors occur when the model fails to comply with the prescribed output syntax, such as missing required actions (No Action) or producing malformed JSON structures (Wrong action format). Each conversation allows a single “thought-only” turn for initial planning, but all subsequent turns are expected to include at least one valid action. Open-source models exhibit notably higher rates of such violations, particularly *Mistral0.3-7B-Instruct* and *InternLM3-8B-Instruct*, which frequently omit or incorrectly format tool calls. In contrast, *GPT-4o* shows substantially fewer syntax-related failures, indicating stronger adherence to structured output specifications. *OPENEARTHAGENT* exhibits the fewest syntax errors overall, suggesting that fine-tuned tool schema conditioning substantially improves output validity.

The reasoning errors are failures in multi-step logic and tool selection, including queries that reach an answer without a single tool call (Ans. w/o tool call) and redundant tool calls in a single step (Multiple tool calls). “Answer w/o tool call” errors are rare across models, showing that most models correctly trigger tools when needed, except *Qwen3-4B-Instruct-2507* and *o4-mini*, which

omit calls more often. Conversely, “Multiple tool calls” are more prevalent, particularly in `Mistral0.3-7B-Instruct`, indicating over-generation and weaker action control. Frontier model (`GPT-4o`) maintains tighter regulation, while `OPENEARTHAGENT` achieves the best balance, invoking tools only when required and avoiding both omissions and redundancies.

S5 Context-Specific Performance Assessment

We further analyze model performance by stratifying the OpenEarthAgent Benchmark across domain-specific categories, including urban planning, environmental monitoring, recreation, industrial infrastructure, disaster assessment, aviation, transportation, and others. This breakdown enables fine-grained evaluation of contextual robustness. Domain-specific difficulty in remote sensing arises from variations in spatial scale, temporal dynamics, spectral ambiguity, and semantic complexity. Structured domains such as urban planning and environmental monitoring typically exhibit stable, large-scale spatial patterns and consistent spectral signatures, making them comparatively easier to analyze. In contrast, disaster assessment involves abrupt temporal changes, heterogeneous damage patterns, and noise, increasing change-detection complexity. Industrial, aviation, and transportation tasks often require fine-grained recognition of small or sparse objects under varying resolutions and viewpoints, demanding stronger contextual and geometric reasoning.

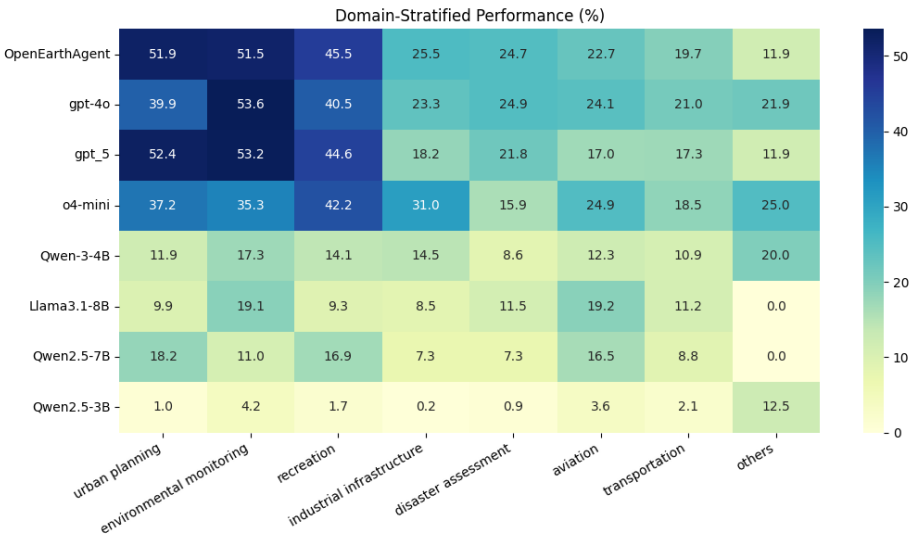


Fig. A2: Domain-stratified performance on the OpenEarthAgent Benchmark. The heatmap shows accuracy across eight geospatial domains. OpenEarthAgent delivers strong, consistent results, particularly in urban planning and environmental monitoring, while remaining competitive in infrastructure and disaster-related tasks.

As shown in Figure A2, OpenEarthAgent demonstrates strong and consistent performance across high-frequency geospatial domains, particularly in urban planning, environmental monitoring, and recreation, where it matches or surpasses frontier models such as GPT-4o and GPT-5. Performance remains competitive in infrastructure and disaster-related tasks, indicating effective generalization to operational geospatial reasoning scenarios. In comparison, open-source baselines exhibit substantially greater performance variance and lower accuracy in complex reasoning tasks.

S6 Qualitative Results

Fig. A3 presents a zero-shot example demonstrating the geospatial reasoning capability of OpenEarthAgent. Given a natural language instruction, the agent autonomously composes a complete multi-step workflow. The agent first formulates a plan to extract the park boundary, compute NBR layers, evaluate their difference, and visualize the result. It sequentially invokes the tools `GetAreaBoundary`, `AddIndexLayer` (for December 2024 and February 2025), `ComputeIndexChange`, and `ShowIndexLayer`, generating a differenced NBR (dNBR) layer that quantifies vegetation loss and recovery. The reasoning trace (middle) of Fig. A3 illustrates coherent tool grounding and correct argument formatting across the entire chain.

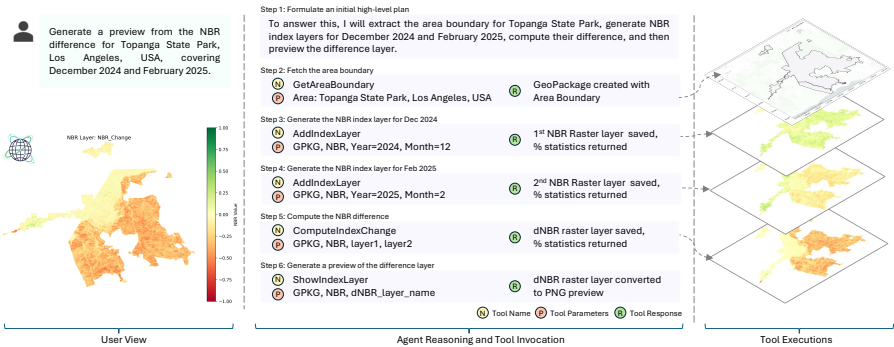


Fig. A3: Example illustrates the zero-shot geospatial reasoning capabilities of OpenEarthAgent on a real-world environmental task by generating a Normalized Burn Ratio (NBR) difference map for a given region. The NBR difference map shows pronounced negative values (red) in southern Topanga, revealing burn scars and vegetation loss, while northern areas remain stable (yellow), showing the post-fire effects from early 2025 events.

Fig. A4 illustrates an example of OPENEARTHAGENT performing metric-scale geospatial reasoning. Given a natural-language query about the distance

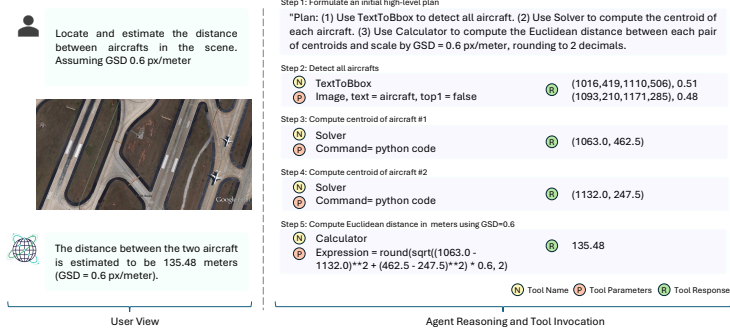


Fig. A4: Example demonstrating OPENEARTHAGENT’s capability for metric-scale geospatial reasoning from imagery, estimating an airplane-to-airplane distance using centroid detection and GSD scaling.

between two vehicles with a GSD of 0.072, the agent composes a workflow: detecting vehicles via `TextToBbox`, computing centroids with `Solver`, and calculating Euclidean distance using `Calculator`. The reasoning trace shows coherent tool use and precise cross-modal computation. In Fig. A5 the agent extracts the buffered area, adds POI layers, computes nearest-neighbor road distances from each kindergarten to the closest police station, and visualizes the POIs and distance links on a base map. This demonstrates the agent’s ability to integrate spatial query and interpretable visualization within a unified reasoning pipeline.

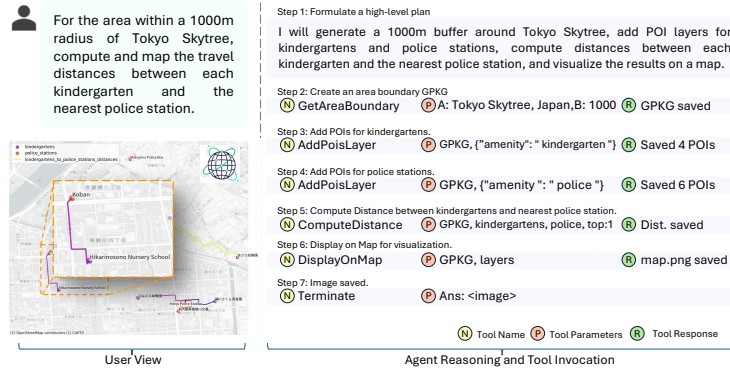


Fig. A5: Example demonstrating OpenEarthAgent’s road-network distance computation and spatial analysis within a 1000 m buffer of a specified area. The visualization highlights the detailed map output generated through sequential tool orchestration.

S7 Tools I/O Structure

The tools used in OpenEarthAgent span a wide range of perceptual, geometric, and analytical operations. They include basic utilities such as drawing boxes, adding text, OCR, and solvers, etc., alongside higher-level tools for object detection, region description, change detection, and pixel-level segmentation. GIS functions such as retrieving area boundaries, adding POI layers, and computing distances, etc., provide the spatial backbone needed for grounded reasoning. Spectral tools further extend this capability by generating and comparing index layers such as NDVI or NDBI. Each tool follows a clear schema with defined inputs and outputs (see Table A8), allowing the agent to compose them into transparent, multi-step reasoning chains across imagery, metadata, and geospatial layers.

S8 Evaluation Prompt

To evaluate the geospatial agent’s final output, we adopt a structured Answer Accuracy assessment framework, illustrated in Fig. A7. The evaluation protocol measures the alignment between a model’s predicted answer and the corresponding ground truth using a normalized score [0,1]. The framework distinguishes between numerical and non-numerical outputs. Quantitative responses are evaluated using a $\pm 10\%$ tolerance threshold, whereas spatial outputs use Intersection over Union (IoU) thresholds. For descriptive or categorical answers, evaluation is based on semantic equivalence, considering paraphrasing, partial correctness, and contradictions. The protocol further defines strict handling of missing, fabricated, or non-responsive outputs, assigning zero scores where required elements are absent or invalid. To standardize assessment, the framework enforces a constrained JSON output format consisting of a numerical score and a concise justification.

S8.1 Open-Source LLM Judge: A Comparative Evaluation

To examine the robustness of our evaluation framework, we replace the original proprietary judge with an open-source model, Qwen3-30B, while keeping the evaluation prompt, scoring criteria, and JSON-constrained output format identical (Fig. A7). This controlled substitution enables a direct cross-judge consistency analysis. As shown in Fig. A6, Qwen3-30B systematically assigns slightly higher absolute Answer Accuracy scores across models. Despite this positive bias in absolute scoring, the relative ranking of models remains preserved, with stronger agents consistently outperforming weaker baselines under both judges. These findings indicate that while Qwen3-30B tends toward more lenient scoring, the structured evaluation prompt ensures consistent comparative trends, demonstrating the robustness of the proposed Answer Accuracy framework across different LLM judges.

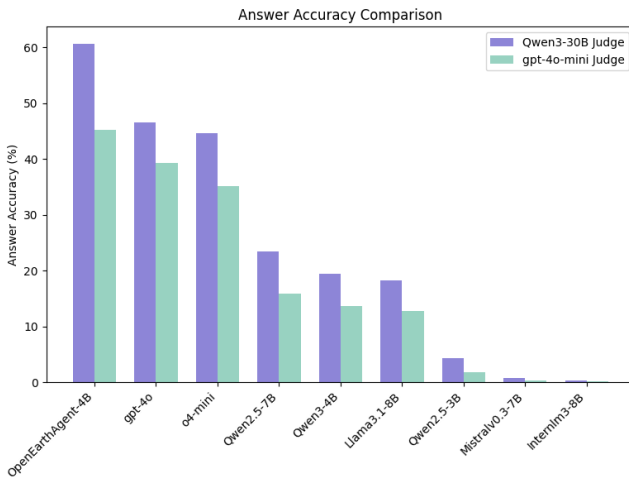


Fig. A6: Evaluation comparison for Geospatial Agent Answer Accuracy Assessment. Although Qwen3-30B assigns slightly higher absolute scores, model rankings remain consistent, demonstrating the robustness of the evaluation framework.

Table A8: List of available tools with brief descriptions, inputs, and outputs.

Tool Name	Description	Input	Output
Calculator	Evaluates math expressions using Python.	Math expression (Python syntax)	Numeric result as text
OCR	Extracts text from an image.	Image	Text with bounding boxes
DrawBox	Draws a box on an image.	Image; box coordinates; optional label	Image with drawn box
AddText	Adds text to an image.	Image; text; position; optional color	Image with text overlay
GoogleSearch	Returns search results from Google.	Query string; optional number of results	Search result text
Plot	Plots data using Python code.	Python code defining <code>solution()</code>	Generated plot image
Solver	Solves equations using <code>sympy</code> .	Python code defining <code>solution()</code> and using <code>sympy</code>	Equation solution as string
TextToBbox	Finds object based on description.	Image; object description	Bounding box coordinates
ImageDescription	Generates a caption for an image.	Image	Text description
RegionAttribute-Description	Describes an attribute in a region or image.	Image; attribute; optional bounding box	Text description of attribute
CountGivenObject	Counts objects in an image.	Image; object name; optional bounding box	Integer count
ChangeDetection	Describes changes between two images.	Text query; pre- and post-images	Description of changes
SegmentObject-Pixels	Segments objects and counts pixels.	Image; object name; optional flag	Pixel count(s)
ObjectDetection	Detects objects in the image.	Image	Labels; boxes; scores
GetAreaBoundary	Gets area boundary as a <code>GeoPackage</code> .	Place name or bounding box; optional buffer	<code>GeoPackage</code> with boundary
AddPoisLayer	Adds POIs to a <code>GeoPackage</code> .	<code>GeoPackage</code> ; query; layer name	Confirmation with POI count
ComputeDistance	Computes distance between layers.	<code>GeoPackage</code> ; source layer; target layer	Summary text and layer name
DisplayOnMap	Renders the map image from layers.	<code>GeoPackage</code> ; layer names	PNG image path
AddIndexLayer	Computes spectral index layer.	<code>GeoPackage</code> ; index type; year; name	Saved layer and class statistics
ComputeIndex-Change	Computes change between index layers.	<code>GeoPackage</code> ; index type; layer names	Saved change layer and statistics
ShowIndexLayer	Generates a preview of the raster index.	<code>GeoPackage</code> ; index type; layer name	Preview image path
GetBboxFrom-Geotiff	Extracts an area bounding box (W,S,E,N) from a <code>GeoTIFF</code> .	<code>GeoTIFF</code>	<code>GeoPackage</code> with boundary
DisplayOnGeotiff	Renders <code>GeoPackage</code> layers (with feature names) over a given <code>GeoTIFF</code> .	<code>GeoPackage</code> ; layers; <code>GeoTIFF</code>	Rendered <code>GeoTIFF</code>
Terminate	Ends task and returns final answer.	Final answer text	None

You are an evaluation assistant responsible for measuring the Answer Accuracy Score (a value between 0 and 1) for a geospatial agent's prediction. You are given:

- A Question
- A Ground Truth Answer
- A Predicted Answer produced by the agent

Your task is to evaluate how accurately the Predicted Answer matches the Ground Truth Answer, considering both numerical precision and semantic correctness. When numerical values are present, allow a $\pm 10\%$ tolerance range for acceptable variation. For descriptive or categorical outputs, judge based on meaningful semantic equivalence.

Evaluation Guidelines

1. Numerical or Quantitative Comparisons

- A predicted numeric value is correct if it lies within $\pm 10\%$ of the corresponding value in the ground truth.
- For bounding boxes, consider the prediction correct if the IoU (Intersection over Union) ≥ 0.5 .
- If multiple numeric values exist:
 - Compute element-wise difference.
 - All values within $\pm 10\%$ range \rightarrow Score = 0.95 - 1.00 (highly accurate)
 - Most values within $\pm 10\%$ range \rightarrow Score = 0.80 - 0.94 (minor acceptable deviations)
 - Some values within $\pm 10\%$ range \rightarrow Score = 0.30 - 0.79 (partially correct)
 - Most values within $\pm 20\%$ range \rightarrow Score = 0.10 - 0.29 (partially aligned)
 - All values incorrect or nonsensical \rightarrow Score = 0.00 (completely incorrect)
- Ignore extraneous numbers that do not directly answer the question.

2. Non-Numerical or Categorical Comparisons

- Evaluate semantic equivalence:
 - Perfect semantic match \rightarrow Score = 1.0
 - Minor phrasing or synonym difference \rightarrow 0.8-0.9
 - Partially correct (missing non-critical details) \rightarrow 0.4-0.8
 - Vague or weakly related \rightarrow 0.1-0.4
 - Contradictory or incorrect \rightarrow 0.0

3. Handling Missing or Contradictory Content

- If the prediction omits all required answer elements \rightarrow Score = 0.0
- If the prediction introduces fabricated entities, relationships, or placeholders \rightarrow Score = 0.00
- If a numeric answer is required and the model responds with "no data", "unknown", or similar \rightarrow Score = 0.00

You must provide your evaluation strictly in the following format and nothing else:

```
{
  "Score": <float between 0.0 and 1.0>,
  "Justification": "<1-2 concise sentences explaining the score based on the comparison between
  GT and Pred>"
}
```

Fig. A7: Evaluation Prompt for Geospatial Agent Answer Accuracy Assessment. The figure shows the structured prompt used to compute an Answer Accuracy Score (0–1) for a geospatial agent's prediction. It defines criteria for numerical tolerance, semantic equivalence, error handling, and required JSON output format for standardized evaluation.